Imaging performance of a dedicated radiation transparent RF coil on a 1.0 Tesla inline MRI-linac

To cite this article before publication: Gary P Liney *et al* 2018 *Phys. Med. Biol.* in press https://doi.org/10.1088/1361-6560/aac813

Imaging performance of a dedicated radiation transparent RF coil on a 1.0 Tesla inline MRI-linac

G.P. Liney[1-4], B. Dong[1], E. Weber[5], R. Rai[1-3], A. Destruel[5], R. Garcia-Alvarez[1], D.J, Manton[1], U. Jelen[1], K. Zhang[1], M. Barton[1-3], P. Keall[6], S. Crozier[5]

[1]Ingham Institute for Applied Medical Research, Department of Medical Physics, Liverpool, Australia.
[2]Liverpool Cancer Therapy Centre, Radiation Physics, Liverpool, Australia.
[3]University of New South Wales, School of Medicine, Sydney, Australia.
[4]Centre for Medical Radiation Physics, University of Wollongong, Australia.
[5]University of Queensland, Biomedical Engineering, Brisbane, Australia.
[6]University of Sydney, ACRF ImageX Institute, Sydney Medical School, Australia.

Corresponding author: A/Prof Gary Liney; gary.liney@health.nsw.gov.au

Purpose: This work describes the first imaging studies on a 1.0 Tesla inline MRI-Linac using a dedicated transmit/receive RF body coil that has been designed to be completely radio transparent and provide optimum imaging performance over a large patient opening.
Methods: A series of experiments was performed on the MRI-Linac to investigate the performance and imaging characteristics of a new dedicated volumetric RF coil: (1) numerical electromagnetic simulations were used to measure transmit efficiency in two patient positions; (2) image quality metrics of signal-to-noise ratio (SNR), ghosting and uniformity were assessed in a large diameter phantom with no radiation beam; (3) radiation induced effects were investigated in both the raw data (k-space) and image sequences acquired with simultaneous irradiation; (4) radiation dose was measured with and without image acquisition; (5) RF heating was studied using an MR-compatible fluoroptic thermometer and; (6) the in vivo image quality and versatility of the coil was demonstrated in normal healthy subjects for both supine and standing positions.
Results: Daily phantom measurements demonstrated excellent imaging performance with stable SNR over a period of 3 months (42.6 ± 0.9). Simultaneous irradiation produced no statistical change in image quality ($p>0.74$) and no interference in raw data for a 20 × 20 cm radiation field. The coil was found to be efficient over large volumes and negligible RF heating was observed. Volunteer scans acquired in both supine and standing positions provided artefact free images with good anatomical visualisation.
Conclusions: The first completely radio transparent RF coil for use on a 1.0 Tesla MRI-Linac has been described. There is no impact on either the imaging or dosimetry performance with a simultaneous radiation beam. The open design enables imaging and radiotherapy guidance in a variety of positons.

Keywords: MRI-Linac, RF coil, Radiotherapy, MRI.

1. Introduction

The pursuit of real-time MR guided radiotherapy has seen the development of several hybrid treatment systems combining an external radiation beam with an MRI scanner [1-3], leading to the first patient treatments on an MRI-Linac system in 2017 [4]. There are two alternative system configurations being investigated, with the radiation beam either perpendicular to, or parallel (inline) with, the main magnetic field. Interactions between the radiation and imaging components depend on both the configuration and magnetic field strength of the MRI-Linac [3].

In MRI, radiofrequency (RF) receiver coils are usually positioned close to the patient in order to maximize the signal-to-noise ratio (SNR) in the acquired image. These coils consist of loops of conductive material and associated electronics (e.g. matching/detuning circuits, preamplifiers) which may be unavoidably placed in the path of the radiation beam in an MRI-Linac. The interaction between the radiation and the RF coil will depend on a number of factors including the design and arrangement of the coil with respect to the beam. This has led several groups to investigate 'beam-on' imaging using both standard and dedicated RF coil designs.

RF coils can be either rigidly made or flexible to better suit anatomy; rigid designs have some advantages for MRI-Linacs as their position with respect to the beam is easier to model and they do not change the patient skin contour. In either case, the materials used in the coil construction will cause attenuation of the radiation beam.

Another consideration is the phenomenon of radiation induced current, whereby an electronic disequilibrium is caused by the ionising beam in conductors or tuning circuits, which has the potential to degrade image quality [5]. Burke *et al.* [6], using specially made 3 & 10 cm diameter solenoid coils, was able to demonstrate a degradation of SNR of 18% with simultaneous irradiation. This effect, which could not be visualised on images but was evident as spikes in raw data (k-space), was found to be related to pulse and echo timings and increased with dose rate. Hoogcarspel et al [7], working on the Utrecht prototype MRI-Linac irradiated a commercial 4 channel flexible RF coil; the primary beam was directed through coil surface but deliberately avoided the electronics housing. This resulted in no measureable change in SNR when a beam on image was compared to imaging with the beam off. The same group repeated their previous study with an anterior and posterior rigid coil combination [8] that consisted of a radio translucent window with the electronics located outside the primary beam. With this arrangement a 5 % SNR loss was measured and beams passing through the posterior coil suffered more than 2 % attenuation of dose.

Liney et al [9] investigated the effects of a 6 MV beam on a 1.5 Tesla clinical scanner. When the integrated transmit/receive body coil was used in conjunction with a radiation field much smaller in size there was no obvious effect on image quality. However, direct irradiation of a 6 channel surface coil produced a 24% increase in background signal.

One final consequence of placing the coil close to the patient is increased surface dose which has been recently shown by Ghila et al [10] to be present irrespective of magnetic field direction. They concluded that standard RF coils should be used with caution and that designs with open 'beam ports' are preferable.

In this study, we characterise the imaging performance of a dedicated RF coil that was designed to work as a combined signal transmitter and receiver on a prototype MRI-Linac system. The coil is completely radio transparent and has neither a dosimetric impact nor effect on image quality during simultaneous irradiation. The first human images obtained using this coil are also presented demonstrating the versatility of the system and its efficacy for MR-guided radiotherapy.

2. Methods

The MRI-Linac (shown in Figure 1 (left)) consists of an integrated treatment delivery system with an open split-bore magnet and imaging hardware described briefly as follows.

The treatment beam is produced by a moveable linear accelerator unit (Linatron, Varex, USA) which can produce photon beams of two energies 4 and 6 MV at two maximum dose rates of 4 and 8 Gy/min respectively. The unit is mounted to a stainless steel table with a clinical 120-leaf (Millennium, Varian) multi-leaf collimator (MLC) in front to provide field collimation. The whole system is mounted on rails, which allows changes of the source to isocentre distance (SID) from 1.9 m to 3.3 m.

A 1.0 Tesla magnet (Agilent, UK) has been designed with a 50 cm gap to permit beam and patient entry in either inline or perpendicular orientations. It is actively shielded to produce a zero Gauss region at 1.2-1.4 m from the isocentre. Imaging gradients are provided by two separate modules (Tesla, UK) that fit in either magnet half with no protrusion into the bore, maintaining the clearance of 50 cm (and 62 cm diameter bore). The gradient coils are capable of amplitudes of 10 mT/m with nominal maximum slew rate of 370 T/m/s. Connections between each module are made at opposite ends (away from the isocentre and RF coil) and cables routed above the magnet at high level.

A novel design was adopted to construct the volume RF body coil (Magnetica Pty Ltd, Australia) while maintaining access from both sides of the central gap and the magnet bore. The geometry of the

RF coil, similar to a four-leg birdcage coil, was fully adapted to the magnet. The design was modelled in FEKO (EMSS, SA), using the method of moments (MoM) and validated experimentally using a mock-up (1:1 scale) of the central gap of the magnet [11]. The RF rungs (copper tubes with inner diameter = 17mm, outer diameter = 19mm, length 480 mm) were aligned along the existing support struts, which connect the two magnet halves through the central gap, creating no additional obstruction as shown in Figures 1 (right) and Figure 2. The support struts of the magnet have been covered with copper cladded polyimide foil. The claddings are connected on both ends electrically to copper cladded flanges. These flanges are attached to the inner faces of the magnet gap, which electrically form the two end-rings of the birdcage-like coil structure. The rungs of the resonator are connected mechanically and electrically (through capacitors) to these flanges. Two opposite rungs are connected to form one channel as shown in Figure 2. A 4-port excitation with active detuning, allowing operation in transmit-only and transceiver mode, was implemented and configured to be fully compatible with the rest of the MRI system. No additional RF-shield was needed. The transceiver body coil is connected to and controlled by a modified (all RF chain retuned to 42MHz) transmit/receive switch and software configuration of an otherwise standard system (Avanto, Siemens Healthcare, Erlangen, Germany). The decoupling of the two channels has been adjusted to be at least -25dB for any loading condition (measured values -31.4dB unloaded and -26.3dB loaded, respectively). Although not described here, as part of system installation, RF tuning calibration for an open, short circuit and 50 ohm termination was performed and was within specifications.

All electronic components are placed well outside of the primary beam (see Figure 2), without affecting the performance of the coil. Images are streamed directly onto the treatment delivery system and used for guidance through the MLC control interface.

The result of using dedicated hardware is an open and patient friendly system with unobstructed views and the flexibility of multiple patient positions for both treatment and imaging. In the current inline configuration a moving patient table is used to position the patient in a perpendicular entry to the magnetic field direction and the beam traverses through a solid hatch in the RF cage wall. This can be removed to enable access to the gradient module, but in normal operation is mounted to maintain the RF integrity of the scan room and consists of approximately 15 mm wood and 1 mm copper thickness [9]. The patient table can be removed completely to allow access to the bore for other positional imaging.

Several experiments were performed to characterise the performance of this open RF coil for the purposes of image guided radiotherapy. These are described as follows:

(i) *Numerical electromagnetic simulations*

The geometry of the RF coil was modelled in Sim4Life (ZMT, Zurich, Switzerland), and was integrated in the magnet gap, represented by its inner flanges. An anatomically accurate model (Duke [12]) was used to simulate the electromagnetic fields for the two subsequent volunteer configurations described in (vi) and shown in Figure 3. Each rung was excited by a 1V voltage source with a 90˚ phase shift between neighbours to simulate the 2 feed ports and half-lambda cables of the real coil. The coil was tuned at 42.0 MHz and the input impedance was matched to 50 Ω with a reflection coefficient better than -20 dB. Decoupling better than -15 dB was achieved between the two channels of the birdcage by using lumped elements in the decoupling rungs. The model was meshed on a non-uniform grid of 107 million cells, with a minimum mesh step of 1.4 mm. Simulations were run using the finite-difference time domain (FDTD) solver, and were allowed to converge to -30 dB. The resulting transmit B_1 efficiency was calculated as $|B_1^+|/\sqrt{P_{in}}$ where P_{in} is the input power in kW.

(ii) *Image quality of the volume RF coil*

Image metrics of SNR and uniformity were measured in a 24 cm diameter floodfill test object containing nickel chloride solution. A spin-echo sequence was acquired (TE/TR = 30/1000 ms) with the phantom at the isocentre and a second repeat image was taken. SNR was calculated from a single region-of-interest by using the mean signal from the first image (S_1) and an estimate of the noise was taken in the same position by measuring the standard deviation (σ_{sub}) in the subtraction of both images [13]:

$$SNR = \sqrt{2}\frac{S_1}{\sigma_{sub}} \qquad (1)$$

Percentage image uniformity (PIU) was measured from the first image using the ACR method [14] which measures mean signal from small regions of interest encompassing areas of greatest (S_{max}) and lowest intensity (S_{min}).

$$PIU = 1 - \left(\frac{S_{max} - S_{min}}{S_{max} + S_{min}}\right) \qquad (2)$$

Lastly, ghosting was assessed by expressing the signal difference between small regions in the phase and frequency direction as a percentage of the mean phantom signal. Images were obtained on a daily basis over a period of 3 months to examine the stability of the imaging system.

(iii) *The effect of the radiation beam on the coil*

In order to examine the possible effect of the radiation beam both raw data (k-space) and reconstructed image data were examined and comparisons made with and without simultaneous

irradiation. The same phantom and set up was used as (ii) and beam on tests were performed with the MLC set to deliver a 20 × 20 cm radiation field at the isocentre using the high energy and dose rate mode. Experiments were carried out with SID = 2.4 m (currently commissioned position). Tests were additionally repeated with the MLC fully retracted in order to examine the extreme case with the radiation field set by the primary collimator in the x-ray head to approximately 50 cm in diameter, and referred to as open field in the following.

Firstly, a specific RF noise acquisition sequence was investigated which utilises no RF pulses (for excitation or refocusing, TE/TR = 1/24 ms) meaning an image is not obtained. This enables any RF interference to be examined in the background without the presence of a large signal. The k-space data was then analysed using a proprietary automatic algorithm (Siemens Healthcare, Erlangen, Germany) which identifies signal that occurs above the noise threshold in either the real or imaginary parts of the data.

The effect of the radiation beam on image space was also investigated; In this case it is appropriate to investigate dynamically acquired scans such as those that would be used during treatment for beam gating and/or tumour tracking. A fast gradient echo sequence (FLASH) was investigated (TE/TR = 10/14 or 50 ms, 25° flip angle) using a 10 mm slice thickness and 2.7 mm in-plane resolution. The temporal resolution of each dataset was 3.3 s or 7.9 s. In each case a total of 75 dynamic images were acquired with the beam turned on during images 25-50 and off at all other times. To analyse these images an alternative multi-acquisition SNR method was used [14, 9] where stochastic pixel variation over time provides an estimate of signal-to-noise:

$$SNR(x,y) = \frac{S_{mean}(x,y)}{\sigma(x,y)} \qquad (3)$$

where $S_{mean}(x,y)$ and $\sigma(x,y)$ are the mean and standard deviations of pixel (x,y) over a finite time period. Pixel-by-pixel maps were produced for each beam on and off interval omitting the first and last images to avoid any transitional effects as the beam is turned on or off. A mean value was then calculated from these maps using a region covering the phantom area.

(iv) *Dosimetry with image acquisition*

In order to rule out the influence of image acquisition on the concurrent dose application, absolute dose measurements were performed. A Farmer-type ion chamber FC65-G (Scanditronix Wellhofer, Uppsala, Sweden), calibrated at 1.0 Tesla and connected to a electrometer (PTW, Freiburg, Germany) with a bias voltage of 300 V. The chamber was placed at the MRI-linac isocentre in a solid water

phantom at a depth of 5 cm with 10 cm of back-scatter material behind. Two series of measurements were performed, during dynamic image acquisition and with no imaging, each consisting of five subsequent irradiations with identical monitor unit settings and a field size of 10 × 10 cm.

(v) *RF heating experiments*

Prior to embarking on volunteer studies an MR compatible fluoroptic thermometer was used to measure any potential heating effects from imaging using this coil. Two independent probes were placed in the centre and surface of a head-sized water filled phantom during a continuous image acquisition of 15 minutes duration. Measurements were additionally taken at various locations within the bore including the surfaces of the RF coil and gradient modules. Skin temperature was also recorded for the first volunteer image examination.

(vi) *In vivo imaging studies*

Two healthy subjects, of different height and weight, were imaged as part of a trial approved by the local hospital ethics committee to demonstrate both the image quality obtained with the coil and the flexibility of patient positioning with the system. In both cases image protocols based on current clinical radiotherapy practice for simulation were used [15]. First, a subject was positioned supine on the patient table and moved into the isocentre and aligned using wall and ceiling mounted lasers projected into the magnet gap. The subject was asked to remain still but no external fixation or other equipment was used. Brain images were acquired in the x-y plane to obtain a sagittal 'beam's eye view' as well as in the z-y plane to obtain an axial image. A T_2-weighted (T_2-w) turbo spin echo (TSE) sequence (TE/TR = 86/5600-13493 ms) was acquired with a 5 mm slice thickness and 1.5-1.8 mm in-plane resolution.

In the second example, the table was retracted, and a different subject was positioned at the isocentre standing upright and facing along the bore in the treatment beam direction. Alignment lasers were used to orientate the subject who was again asked to remain still during the scan. In this case a lumbar spine image was acquired in the sagittal plane using a T_2-w TSE sequence (TE/TR = 86/3200 ms) with a 5 mm slice thickness and 1.5 mm in plane resolution with a 30 × 30 cm field-of-view (FOV). All images were subjectively reviewed by an experienced radiotherapy radiographer (RR) for overall quality, presence of artefacts and anatomical visualisation from the perspective of use in treatment planning.

3. Results

The simulation experiments showed that when the coil was loaded with the head in the FOV, the transmit efficiency (mean ± standard deviation) in the brain tissues was 6.75 ± 0.18 μT/√kW. When the coil was loaded in the standing upright position (Figure 4), the simulated transmit efficiency in the human tissue inside the 30 cm DSV system specification was 6.25 ± 0.29 μT/√kW. Corresponding values for larger DSV were 6.32 ± 0.32 μT/√kW and 6.46 ± 0.39 μT/√kW at 40 cm and 50 cm respectively.

Figure 5 (a) shows an example image of the phantom obtained with the RF coil as part of the daily quality assurance of the system. The Q factor of the coil loaded in this manner was 45 (corresponding unloaded value was 58). The image is displayed in two halves using separate window width/level settings in order to visualise both the signal and background. Image uniformity was 64 % and SNR was measured as 42.6 ± 0.9 (mean ± SD) over a period of 3 months. Ghost levels were not detectable within a 2.5 % accuracy.

Examination of the k-space data from the noise acquisition sequence showed no difference between beam on and off when using a 20 × 20 cm radiation field. In the case of an open radiation field a single low intensity spike was detected (Figure 5 (b)). Although this is an extremely minor interference, the test was repeated a second time which confirmed that the artefact was due to the presence of radiation.

The dynamic images did not exhibit any changes in phantom signal or background signal with the beam on in any of the tests. Figure 5 (c) shows a plot of the background signal intensity in each image together with the mean values for the beam on and off intervals. No statistical difference between the 'on' and 'off' intervals was found in any of the experiments using unpaired t-tests (equal variances) with $p=0.747$ and $p=0.883$ for 20 × 20 cm and open field respectively. Table 1 gives the mean values of pixel-by-pixel SNR for each experiment and for each individual beam on and beam off period. The changes observed when the beam is turned on are negligible: the values are within the variation of the mean SNR variation that occurs without the irradiation.

As expected, there was no impact from the imaging on dose delivery with the mean (± SD) dose of 1.053 (± 0.001) Gy recorded during continuous image acquisition compared to 1.053 (± 0.002) Gy without imaging.

Temperature measurements during the extended 15 minute image acquisition demonstrated only small changes (+0.3 °C on the surface and -0.3 °C at the centre) in the water phantom. Larger temperature increases were found to occur on the surfaces of the RF rungs (+2.1 °C) and the gradient modules (+10.8 °C) over the same 15 minute period, with no part of the gradient module exceeding 31.3 °C. Subsequently, no measurable change in skin temperature of the volunteer could be detected.

Figure 6 shows photographs and example images acquired in the healthy volunteer study. In both cases, the open aperture created by the RF coil (black rungs) can be seen in the first photograph and the coil is completely hidden from view in the second photograph taken down the bore. Note also that nothing is placed on or near the subjects and all imaging was obtained with the open RF coil only. In Figure 6 (a) a female subject (height 153 cm, weight 53 kg, BMI 23.1) is positioned supine in the magnet gap to obtain brain images acquired in 4.5 minutes. The sagittal T_2-w image shows excellent grey-white matter differentiation and ample coverage of the entire skull and lower portion of the cervical spine with no distortion of the anatomy at the peripheral field of view. There is clear visualisation of the corpus callosum, brain stem and spinal cord as well as sinus cavities. The overall signal intensity and normalisation is homogenous with no artefacts obstructing visualisation of brain structures. The axial T_2-w image again shows excellent contrast-to-noise ratio with grey-white matter differentiation and high signal in the cerebrospinal fluid (CSF). There is clear visualization of lateral ventricles and subtle visualisation of the caudate nucleus, putamen, thalamus and the internal and external capsules.

Figure 6 (b) illustrates the standing position that is possible on this system with a second male subject (height 180 cm, weight 90 kg, BMI 27.5). The sagittal T_2-w lumbar spine image, which was acquired in 2 minutes, has excellent contrast-to-noise ratio with excellent visualisation of all structures including the conus, cauda equina, CSF, intervertebral discs and vertebral bodies. It was also noted that there are minimal breathing and motion artefacts impacting the visualisation of the spinal column, while the subject is in the erect position.

4. Discussion

The use of an RF coil in an MRI-Linac requires careful consideration with respect to its operation with a simultaneous radiation beam. The normal requirement of coil proximity to the patient to achieve high SNR in diagnostic imaging has to be weighed against the possible interactions with the treatment field on a hybrid treatment system. Depending on the design of the coil, some or all of the planned radiotherapy beams may pass through the coil affecting the intended dose. In turn, the radiation can cause interference in the received signal leading to reduced SNR. This work describes, for the first time, a dedicated open coil that was designed in order to have no impact on either the dosimetric or imaging performance during irradiation on a 1.0 Tesla inline MRI-Linac.

The RF coil is efficient and compares favourably with standard clinical body coils [16]. It provides good quality artefact free images, with and without the presence of the radiation beam, and has demonstrated a stable performance over time. We examined the possibility of radiation induction effects in both raw data and magnitude reconstruction images. Firstly, a sequence was acquired without RF pulses in order to examine the noise. The operation of the beam with a 20 × 20 cm radiation field did not show any evidence of interference. Even in the extreme case of a non-collimated radiation field there was only a single minor spike detected which is atypical of radiation interference described to date [6,8,9]. During dynamic image acquisition we were unable to detect any statistical difference in signal with the radiation beam turned on in any of the tests. We conclude that the radiation has no effect on the images acquired with this coil. The physical opening that the coil provides also means there is no attenuation of the treatment dose and this was confirmed by ionisation chamber measurements with and without image acquisition. These results represent an improvement compared to coils that have been previously described for MRI-Linac systems [6,8,9].

Although this was not tested in the current study, considering there are no RF coil conductors in the perpendicular aperture of 50 × 78 cm, it is likely that the coil would also be radio transparent in this direction and could be investigated in future. Of course, this only applies to a non-rotating system; in future we intend to maintain a fixed beam geometry by either rotating the whole MRI-Linac assembly, or, moving the patient [17].

The first in vivo images of the system were also acquired and have demonstrated sufficient image quality for treatment guidance especially considering the absence of any secondary coil placed on the subject. Volunteer imaging has been well tolerated with no adverse effects; the minimum magnetic field excursion required for stimulation extrapolated to a zero rise time exceeds what is possible with the current gradient specification [18]. No significant RF heating has been measured for the specific

sequence reported and further studies will be performed to provide a thorough assessment for other imaging orientations.

The versatility of this coil design has also been shown with imaging in two different positions, using two physically different subjects, including the first stand-up images acquired on an MRI-Linac system. This may have a number of advantages over more conventional treatment positions and will be the subject of further investigations.

5. Conclusion

In conclusion, we have characterised the imaging performance of a novel volumetric transceiver RF coil for use in a 1 Tesla inline MRI-Linac. The coil provides good image quality with no mutual interaction with the radiation beam, while maintaining an open and versatile patient environment. The coil may also be used in transmit mode, and we are currently working on other open designs of receiver-only coils for specific applications.

Acknowledgements

This work has been funded by the Australian National Health and Medical Research Council Program Grant APP1132471.

6. References

[1] B. W. Raaymakers et al. Integrating a 1.5 T MRI scanner with a 6 MV accelerator: proof of concept. Phys Med Biol, 54(12):N229237, 2009.

[2] B.G. Fallone, B. Murray, S. Rathee, et al. First MR images obtained during megavoltage photon irradiation from a prototype integrated linac-MR system. Med. Phys. 36, 2084−2088, (2009).

[3] P.J. Keall, M. Barton, S. Crozier. The Australian magnetic resonance imaging-linac program. Semin Radiat Oncol 24, 203-205 (2014).

[4] B. W. Raaymakers et al. First patients treated with a 1.5 T MRI-Linac: clinical proof of concept of a high-precision, high-field MRI guided radiotherapy treatment. Phys Med Biol.2017;62(23): doi: 10.1088/1361-6560/aa9517.

[5] Burke B, Fallone BG, Rathee S, 2010 Radiation induced currents in MRI RF coils: application to linac/MRI integration. *Phys Med Biol* 55;735-746.

[6] B. Burke et al. Effect of radiation induced current on the quality of MR images in an integrated linac-MR system. Med Phys 2012; 39(10): 6139- 6147.

[7] S.J. Hoogcarspel et al. The feasibility of using a conventional flexible RF coil for an online MR-guided radiotherapy treatment. Phys Med Biol 2013; 58:1925-1932.

[8] S.J. Hoogcarspel et al. Characterization of the first RF coil dedicated to 1.5 T MR guided radiotherapy. Phys Med Biol 2017; in press.

[9] G.P. Liney et al. Experimental results from a prototype high-field MRI-Linac. Med Phys 2016; 43: 5188-5194.

[10] A. Ghila, B.G. Fallone, S. Rathee. Influence of standard RF coil materials on surface and buildup dose from a 6 MV photon beam in magnetic field. Med Phys.2016;43(11): 5808.

[11] A. Destruel, E. Weber, I. Hughes, Y. Li, F. Liu, S. Crozier. Design of a whole-body radiofrequency coil for image-guided radiotherapy treatment in a MRI-Linac system. 2015; 3076 Proc. of ISMRM

[12] M.C. Gosselin et al. Development of a new generation of high-resolution anatomical models for medical device evaluation: the Virtual Population 3.0. Physics in Medicine and Biology 2014;59(18):5287-5303.

[13] O. Dietrich, J.G. Raya, S.B. Reeder, M.F. Reiser, S.O. Schoenberg. Measurement of signal-to-noise ratios in MR images: influence of multichannel coils, parallel imaging, and reconstruction filters. J Magn Reson Imaging 2007;26:375–85.

[14] American College of Radiology, Magnetic Resonance Imaging Quality Control Manual (American College of Radiology, Reston, VA, 2004).

[15] G.P. Liney, M.A. Moerland. Magnetic resonance imaging acquisition techniques for radiotherapy planning. *Semin Radiat Oncol* 2014; 160-168.

[16] O. Weinberger et al. Local mutli-channel RF surface coil versus body RF coil tranmisssion for cardiac magnetic resonance at 3 Tesla: Which configuration is winning the game? PLOS ONE DOI:10.1371/journal.pone.0161863

[17] B.M. Whelan, et al. An MRI-Compatible patient rotation system - Design, construction, and first organ deformation results. Med Phys. 2016, doi: 10.1002/mp.12065.

[18] D.W. McRobbie, 'Bio-effects of Gradient Magnetic Fields' in Magnetic Resonance Procedures: Health Effects and Safety (Ed Frank G. Shellock and John V. Crues, III), Los Angeles: Biomedical Research Publishing Group), 2013.

Table 1: Mean values taken from pixel-by-pixel SNR maps (see Figure 2 (d)) calculated for each of the beam on and beam off intervals.

Radiation field	Repetition time (TR)	Beam Off	Beam On	Beam Off
20 × 20 cm	14 ms	30.0	30.1	30.2
20 × 20 cm	50 ms	46.9	46.9	47.1
Open	14 ms	30.4	30.3	30.0
Open	50 ms	46.8	46.8	47.0

Figure 1: (left) Photograph showing the linear accelerator and MLC inline with the magnet. In normal operation the beam traverses a solid RF panel which has been removed to show inside the magnet bore. (right) View from the side of the magnet with the table retracted showing the two gradient modules (GM) and RF coil (RF) in the patient gap. The support struts of the magnet can be also seen and these are covered with copper polyimide foil.

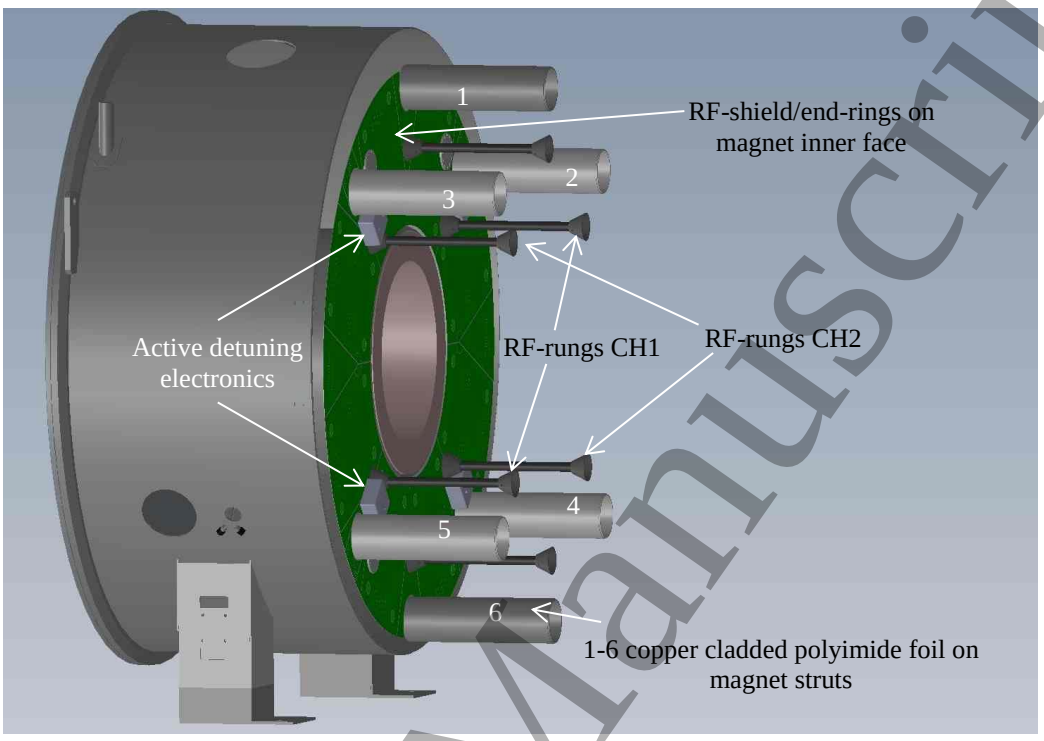

Figure 2: Structure and main components of RF body coil (one half of the system shown). The copper cladded magnet support struts (1-6) and the RF-shield/end-rings mounted on the magnet inner faces form the semi-open RF shield. Active detuning circuitry is implemented on each of the four main RF rungs of channels CH1 and CH2 (only two are labelled).

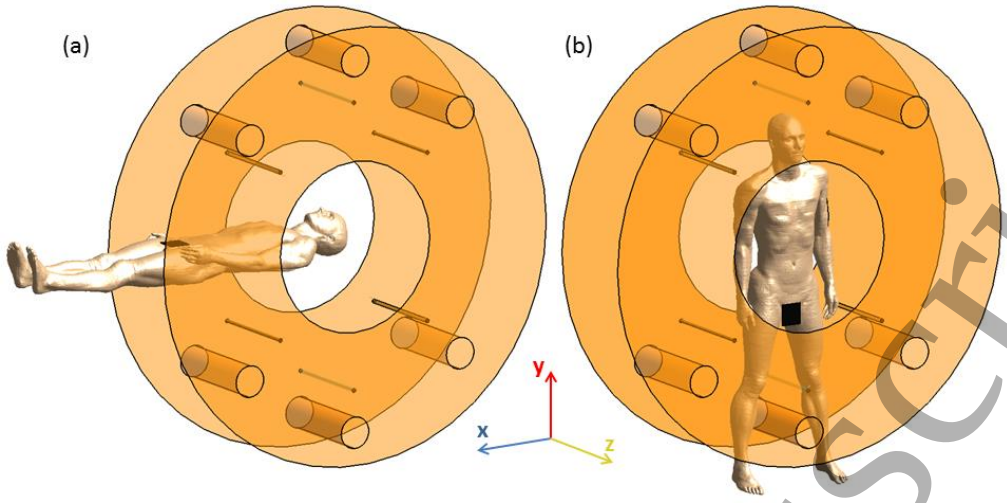

Figure 3: Model of the RF coil inside the magnet gap loaded with (a) patient with a perpendicular entry in a supine position with the head in the isocentre; (b) patient standing upright facing along the magnetic field direction with the spine at the isocentre.

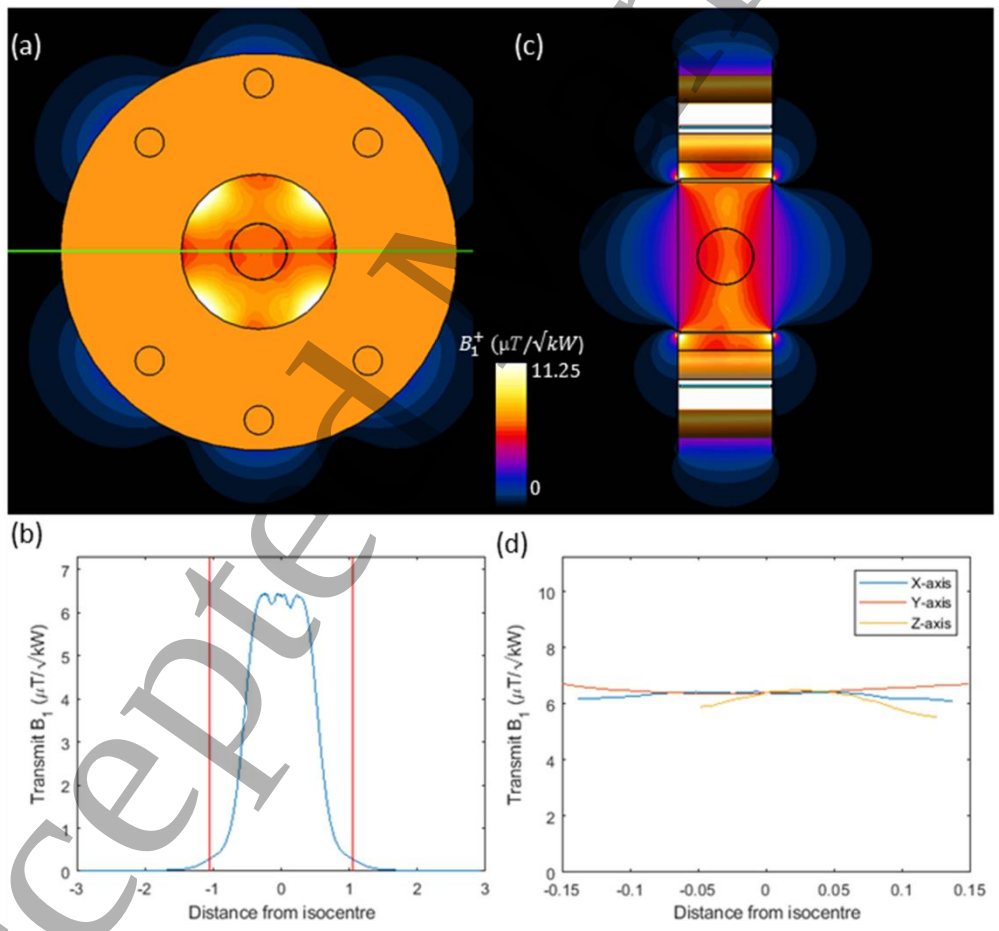

Figure 4: (a) Slice of the transmit efficiency in the centre xy-plane of the magnet, loaded in standing position. The dark circle shows the 30 cm DSV. The field along the green line is plotted in (b). The two vertical lines show the end of the flanges of the magnet gap. (c) Slice of the transmit efficiency in the centre yz-plane. (d) Plot of the transmit efficiency in Duke inside the DSV along the three axes.

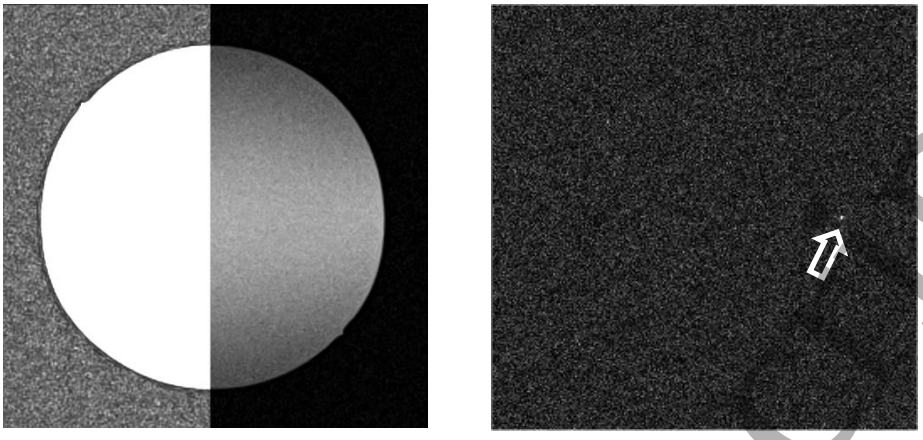

Figure 5: (a) Example of a daily quality assurance image of the RF coil with no radiation beam; the image is shown in two halves with different window settings to visualise signal in the phantom and background. **(b)** k-space data acquired with no RF pulses and simultaneous irradiation to examine presence of radiation induced current. Even in this case of an open radiation field there is a negligible effect and only one minor signal spike could be detected (arrow).

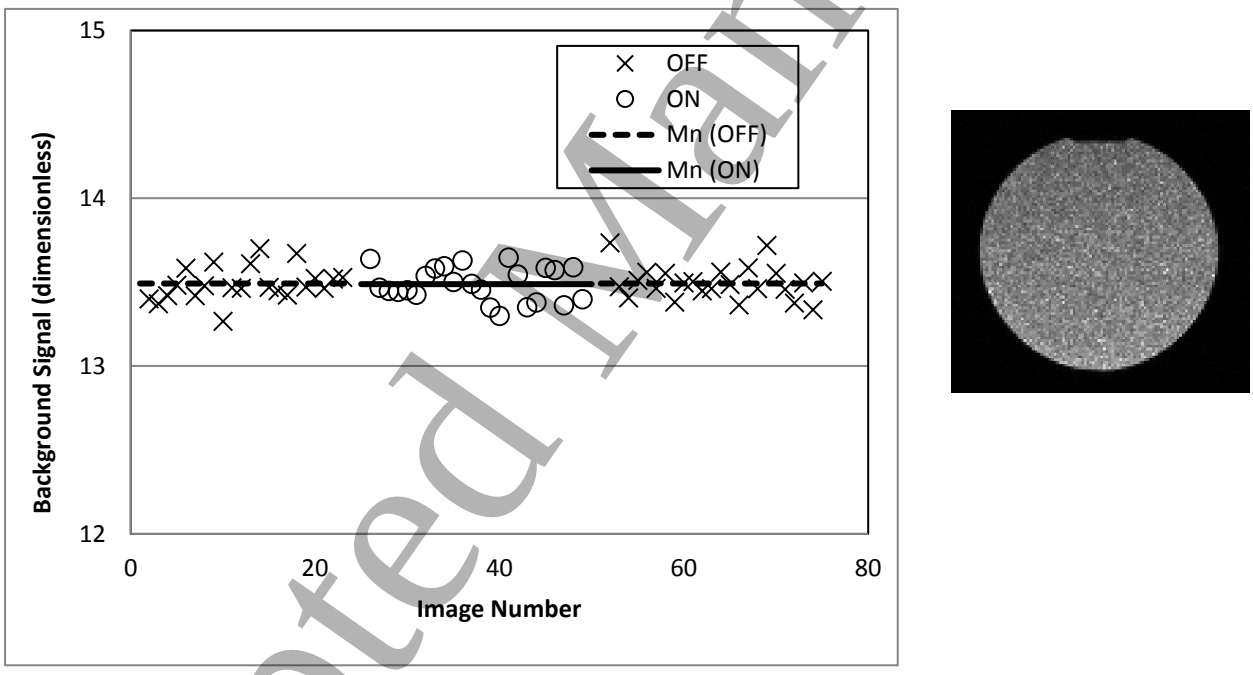

Figure 5: (c) Plot of the background signal during the dynamic acquisition of the TR = 50 ms sequence. The radiation beam is turned on with an open field during images 25 to 50 (circles) and is off at other times (crosses); the horizontal lines show the mean value over each interval. **(d, inset)** Example map of SNR generated from pixel-by-pixel variations (using equation 3) over specific time intervals and used to compare beam on versus beam off.

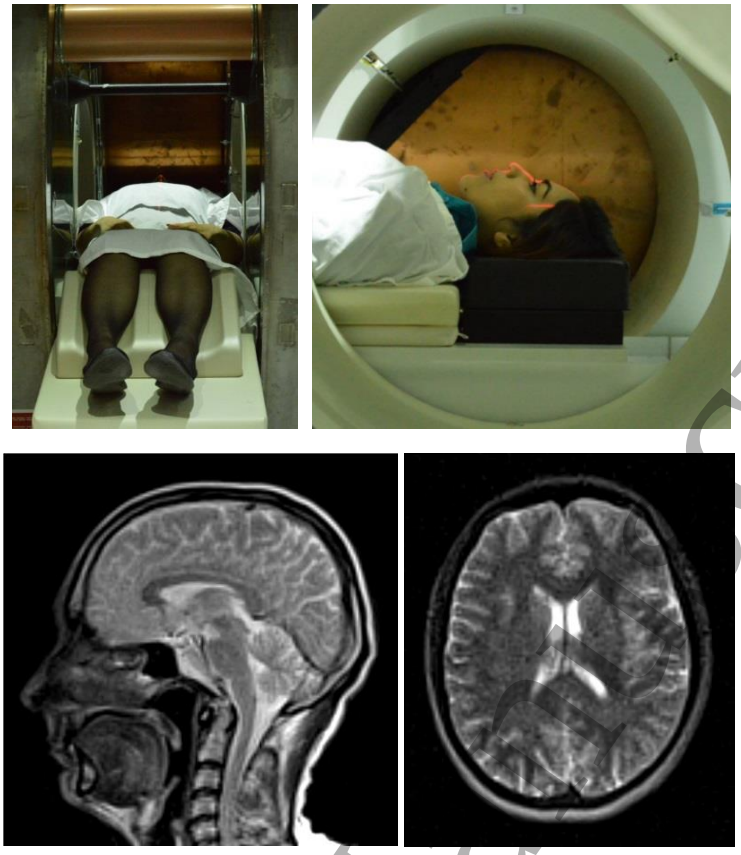

Figure 6 (a): (top) Photographs illustrating the subject lying supine on the patient table with a perpendicular entry into the magnet. (bottom) Example T_2-w brain images acquired in the sagittal and axial planes with the subject in the position shown.

Figure 6 (b): (left & centre) Photographs of a subject standing upright in the magnet isocentre facing in the direction of the beam/magnetic field. (right) A T_2-weighted sagittal lumbar spine image acquired with the subject in this position.